Mars and Earth Upper Atmosphere Sensing Simulations of Rayleigh and Na Resonance Lidar from Spacecraft

G. Swenson[(1)], P. Dragic[(1)], L. Waldrop[(1)], J. Plane[(2)], Chad Carlson[(1)], and A. Liu[(1)]
[(1)]*University of Illinois, 1308 W. Main, Urbana, Il, 61801, USA, swenson1@uiuc.edu*
[(2)]*University of Leeds, School of Chemistry, University of Leeds, Leeds LS2 9JT, UK, j.m.c.plane@leeds.ac.uk*

ABSTRACT

The investigations of the dynamics of the upper atmospheres of both Mars and Earth involve the measurement of a large range of wave scales including planetary waves, tides, and atmospheric gravity (buoyancy) waves (AGWs). Tides and AGWs are of particular interest in the 40-120 km region of both planets. In particular, AGWs play a large role in the local accelerations of the mean flows as they dissipate and break. The transport of energy and momentum in AGWs contributes to large affects on the mean flows and densities which affects aero-braking and re-entry vehicles.

The evolution in solid state laser transmitters opens the consideration to develop lidar investigations of the upper atmosphere waves using lidar from 'dipper' orbits. Simulations of the S/N for both Na resonance and Rayleigh lidar for upper atmospheric measurements of Mars with comparisons to Earth simulation results are described.

1. BACKGROUND

Mars and Earth atmospheric observations from spacecraft have a long history of passive remote sensing from low altitude, circular orbits above 500 km which have relatively long orbital lifetimes (years) without boost. Aero-braking orbits have been considered and flown on Earth, but recent successes on Mars, such as the 2001 Odyssey spacecraft, use an aero-braking (ABO) or 'dipper' orbit with perigee ~135 km, for a period of ~ 6 months.

In this simulation, we have considered the aero-braking orbit phase of Mars missions, and performed simulated returns for lidar remote sensing in the 40-130 km regions of the atmosphere using both Rayleigh, at 355 nm, and Na resonance lidar at 589 nm.

The Mars atmospheric mass density is about the same as the Earth's atmosphere at 120 km. Considering the atmospheric temperatures and scale heights, the Mars atmosphere is less dense than Earth's below this altitude, and greater, above this altitude. It has been assumed that the meteor flux at Mars is similar to that of Earth which populates the upper atmosphere with a metals layer. The presence of the atomic species (i.e. Na, Fe, Mg, etc.) density/altitude distributions depend on post ablation chemistry and vertical mixing through atmospheric diffusion (eddy, wave, and molecular). The Mars atmospheric layers are low in altitude and spread over a broader altitude region than on Earth.

The development and evolution of solid state, fiber amplifier laser system technology, combined with the success of aero-braking satellite missions provide the incentive to consider this approach to remotely sense the large variability caused by small scale waves on global scales.

2. RAYLEIGH LIDAR CONSIDERATIONS

Lidar Equation, # photoelectrons produced from range element

transmitted photons

Receiving probability

$$N(z) = \{\eta T_A^2\}\left\{\frac{P_L \tau}{h \cdot c/\lambda}\right\}\{\sigma_{eff} \cdot n_s(z) \cdot \Delta z\}\left\{\frac{A_R}{4\pi z^2}\right\} + N_B R \tau$$

System efficiency/ atmospheric transmission

Scattering probability

Background

$\sigma_{CO2,RayBS}$=6.36 10^{-32} m^2 str^{-1}
(Shardanand and Rao, 1977)
$\sigma_{Na,Flour}$=1.3 10^{-15} m^2
(McIlrath, 1980)

S/N = $\sqrt{N(z)}$
{S/N shown assumes zero background, i.e. night time}

Fig 1. Lidar equation for both Rayleigh and Na resonance used for the simulations described. Cross sections for the Mars CO_2 [1] and Na [2] are shown.

The lidar equation describing the signal return for a given transmitter power is shown in Fig 1. The Rayleigh cross section for the Mars atmosphere, which is dominated by CO_2, is approximately 3 times larger than what it is on Earth (for an N_2 and O_2 atmosphere).

The model atmosphere used for the Rayleigh simulations is shown in Fig. 2 [3] [4].

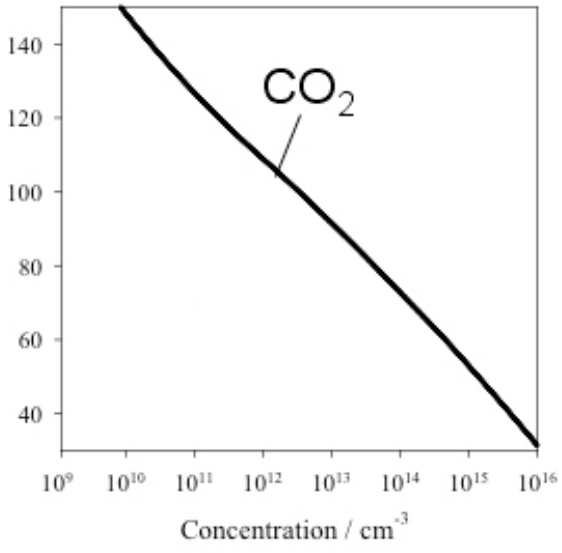

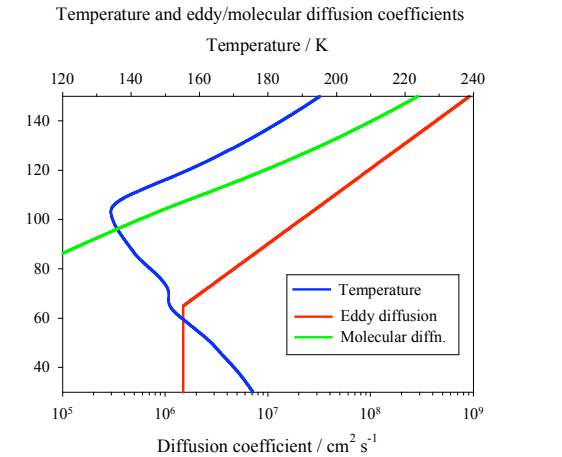

Fig 2. Top. Composition model for consideration of the Rayleigh scatter return for the Mars lidar

The baseline lidar configuration for the simulations were a 10 W (average power) Master Oscillator Power Amplifier (MOPA) fiber laser, with a 1 m diameter mirror, with a system optical efficiency of 10%.

The Signal to Noise ratio (S/N) calculations were made with the above transmitter/receiver, with a combined integration time (IT) product with the range bin (Δz) of 60 km s^{-1} (e.g. 1 km range bin for 60s, or 10 km range bin for 6 s). On Mars the orbital velocity of the spacecraft is ~ 4 km s^{-1}. The S/N calculations then represent a spatial volume (Δz x Δh), where h is horizontal distance along the orbital trajectory path, of 1 x 240 km^2 or 10 x 24 km^2. In this simulation, the S/N considers only the signal return which is assumed Poisson distributed, with zero background or sensor dark count, where S/N = √S. These are considerations which could be achieved for night time sampling of the Mars atmosphere. Since the S/N = √S, the scaling of larger or smaller integration volumes are readily scaled from the simulation results.

Fig. 3 describes the results of the Rayleigh return for the system.

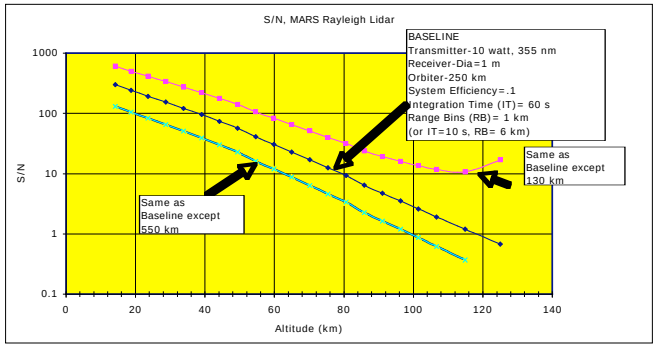

Figure 3. S/N for the Baseline lidar for a Mars atmosphere vs. altitude. The S/N is shown for measurements from 550, 250, and 130 km altitude.

Dust particles in the Martian atmosphere were assumed to be spherical grains with an effective radius of 1.5 +/- 0.2 um and a complex index of refraction of 1.5 + 0.004i. A model of the dust distribution in altitude was adapted from [4], with a surface density of 0.6 cm-3 [5] and a maximum altitude extent of 50 km. The relative Mie to Rayleigh returns for the nominal model are shown in Fig. 4.

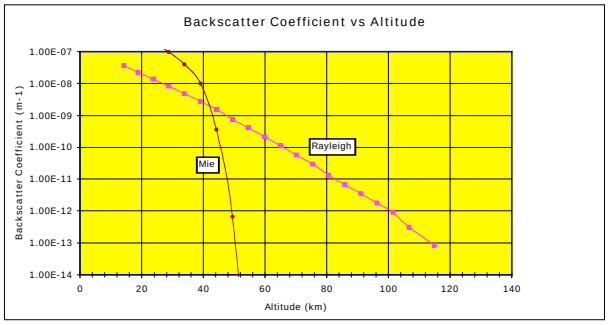

Fig. 4. The relative backscatter return from an assumed dust model vs. a Rayleigh backscatter.

The relevance here is that below 50 km, the lidar returns would be from dust and dust distributions can be measured, but more importantly, this denotes the lower limit of Rayleigh returns.

In Fig. 5, the Rayleigh return has be downward integrated using the hydrostatic gas low, and the S/N is shown for both a Mars orbiter (at 130 km) and Earth (at 130 km).

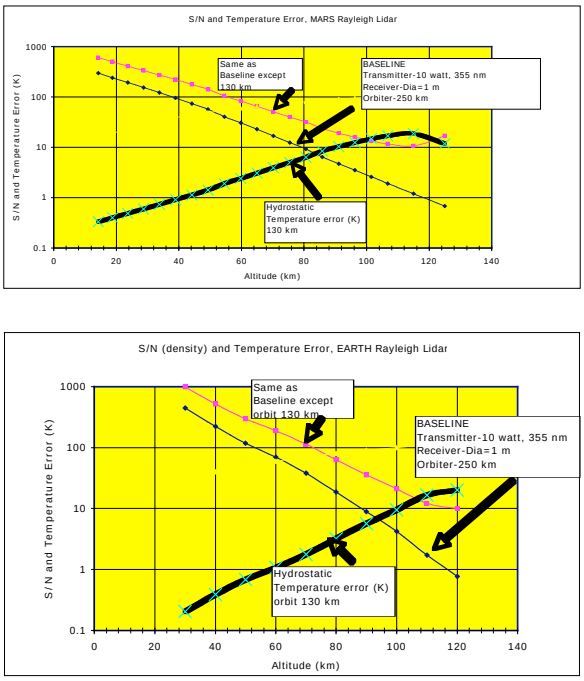

Fig. 5. S/N for Rayleigh determined hydrostatic temperature vs altitude for Mars (top) and Earth (bottom) for 130 km orbiter altitude.

3.LIDAR DESCRIPTION

A cross section of the lidar system is shown in Fig. 6.

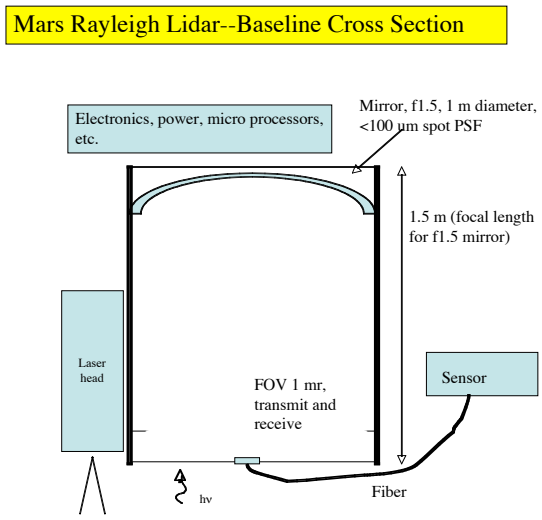

Fig. 6. A system schematic describing the basic elements used in the simulation.

The heart of the system is the transmitter which is schematically shown in Fig. 7.

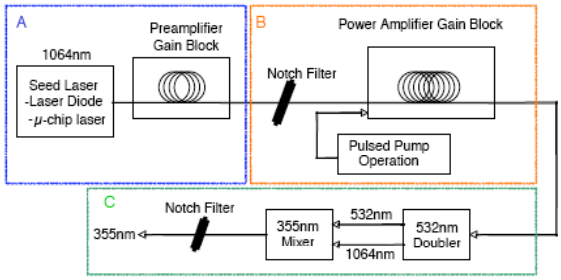

Fig. 7. A block diagram showing the elements of a solid state MOPA laser configuration capable of meeting the specifications of the Mars lidar described here.

The UV transmitter basic properties include a PRR of 1 kHz, with six pulse outputs, 10 ns each, separated by 1 μs, with a total pulse duration of 6.6 μs, a range bin of ~ 1 km, with a spectral width of <10 GHz.

The power amplifier is a six element, sequentially-fired Yb-doped fiber amplifier [5] array employing a pulsed pumping platform [6] to achieve the low PRR. 300 W peak pump power employing end pumping/fiber pump combiners, with 50 μs pump pulse width, will yield an average pump power per element of 15 W. We anticipate ~ 180 W heat to be dissipated through passive coupling. The 500 kW peak power from a single Yb power amplifier stage, is Raman limited [7]. We expect 5 W average power for each element, times six elements for a total of ~30 W average power. This

output will be frequency tripled, with ~ 1/3 efficiency, using nonlinear crystals [8]

The wall-plug efficiency of >3% into the UV, 10 W average power is the design goal and expectation. It is anticipated that the lidar would be operated ~10% of an orbit time so that the average operating power would be compatible with a typical spacecraft power budget. Certainly in the aero-braking phase of a mission, this would be the fraction of operating time which would yield a practical (valuable) return.

4. AN Na RESONANCE CALCULATION

A Mars model for the vertical distribution of Na from meteor oblation was also developed. The very large resonance return is described in Fig. 8. Both the S/N of signal returns from a 10 W Na resonance and a 10 W Rayleigh system are shown. Here, the S/N is assuming, for Na, the laser power is distributed over the center _ of the population distribution for resonance considerations. The S/N will provide a reference for the vertical distribution of Na density, which contains the constituent redistribution (or footprint) of the vertical winds associated with high frequency AGWs.

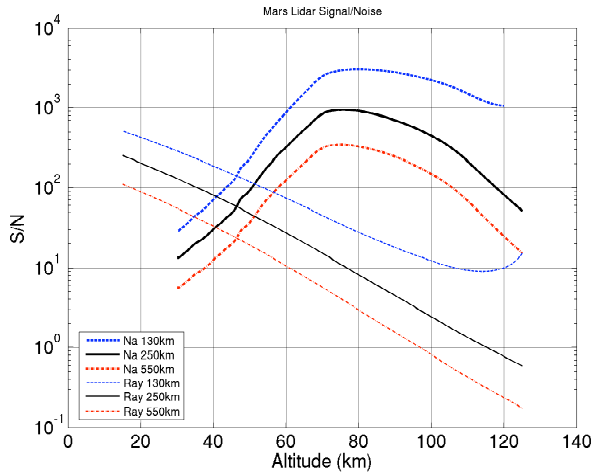

Fig 8. The S/N of lidar signal returns vs. altitude, for Na and Rayleigh, for a Mars lidar, for 3 reference altitudes of the spacecraft.

5. Summary

Tides and AGWs in the Mars upper atmosphere can be measured through their perturbations to the density, temperature, or wind field. The Rayleigh method demonstrated a >10 S/N for 40-120 km for 130 km 'dipper'. The Na lidar would provide a S/N of >100 over most of the range from 550 km, which would be a nominal, circular orbit for long term studies of the atmosphere.

Laser transmitter evolution is expected to be able to deliver pulsed powers with the described spectral attributes in the next few years, and as they do evolve, the capabilities to make the described measurements will be possible.

6. References

1. McIlrath, T. J. "Fluorescence Lidar", Optical Engineering, 19, 494-502, 1980

2. Shardanand, A. D. and P. Rao, Absolute Rayleigh Scattering Cross Sections of Gases and Freons of Stratospheric Interest in the Visible and Ultraviolet Regions, NASA TN O-8442, 1977

3. Forget F. et al., J. Geophys. Res., 104, 24155, 1999.

4. Justus, C. G., et al. , Mars-GRAM 2000: A Mars Atmospheric model for Engineering Applications, Advances Space Res., 29, 193-202, 2002

5. Korablev, O.I., V.A Krasnopolsky, A.V Rodin, and E. Chassefiere, "Vertical structure of Martian dust measured by solar infrared occultations from the PHOBOS spacecraft", Icarus, v. 102, pp. 76-97, 1993.

6. Paschotta, R., J. Nilsson, A.C. Tropper, and D.C. Hanna, "Ytterbium-Doped Fiber Amplifiers," *IEEE Journal of Quantum Electronics*, vol. 33, no. 7, July 1997, pp.1049-1056.

7. Swenson, G. R., P.D. Dragic, and A.Z. Liu, "A high power Rayleigh lidar for measurement of upper atmospheric temperature and geostrophic winds," paper presented at CEDAR NSF Workshop, Santa Fe, NM, June 26-30, 2004.

8. Agrawal, G. P., *Nonlinear Fiber Optics*, Academic Press, 1995.

9. Kliner, D. A. V., F. DiTeodoro, J.P. Koplow, S.W. Moore and A.V. Smith, "Efficient second, third, fourth, and fifth harmonic generation of a Yb-doped fiber amplifier," *Optics Communications*, vol. 210, 15 September, 2002, pp. 393-398.